Appl Nanosci (2016) 6:485–494
DOI 10.1007/s13204-015-0453-3

ORIGINAL ARTICLE

The effect of solution pH on the electrochemical performance of nanocrystalline metal ferrites MFe_2O_4 (M=Cu, Zn, and Ni) thin films

E. M. Elsayed[1] · M. M. Rashad[1] · H. F. Y. Khalil[2] · I. A. Ibrahim[1] · M. R. Hussein[1] · M. M. B. El-Sabbah[2]

Received: 22 January 2015 / Accepted: 23 April 2015 / Published online: 16 May 2015

Abstract Nanocrystalline metal ferrite MFe_2O_4 (M=Cu, Zn, and Ni) thin films have been synthesized via electrodeposition–anodization process. Electrodeposited (M)Fe_2 alloys were obtained from aqueous sulfate bath. The formed alloys were electrochemically oxidized (anodized) in aqueous (1 M KOH) solution, at room temperature, to the corresponding hydroxides. The parameters controlling the current efficiency of the electrodeposition of (M)Fe_2 alloys such as the bath composition and the current density were studied and optimized. The anodized (M)Fe_2 alloy films were annealed in air at 400 °C for 2 h. The results revealed the formation of three ferrite thin films were formed. The crystallite sizes of the produced films were in the range between 45 and 60 nm. The microstructure of the formed film was ferrite type dependent. The corrosion behavior of ferrite thin films in different pH solutions was investigated using open circuit potential (OCP) and potentiodynamic polarization measurements. The open circuit potential indicates that the initial potential E_{im} of $ZnFe_2O_4$ thin films remained constant for a short time, then sharply increased in the less negative direction in acidic and alkaline medium compared with Ni and Cu ferrite films. The values of the corrosion current density I_{corr} were higher for the $ZnFe_2O_4$ films at pH values of 1 and 12 compared with that of $NiFe_2O_4$ and $CuFe_2O_4$ which were higher only at pH value 1. The corrosion rate was very low for the three ferrite films when immersion in the neutral medium. The surface morphology recommended that Ni and Cu ferrite films were safely used in neutral and alkaline medium, whereas Zn ferrite film was only used in neutral atmospheres.

Keywords Ferrites · Nanoparticles · Corrosion · pH · Polarization curves

Introduction

Spinel ferrite materials MFe_2O_4 (M = divalent metal ion such as Mg, Mn, Ni, Fe, Cu, Co, etc.) are the most versatile materials because of their wide range of technological applications in various areas such as biomedicine, magnetic resonance imaging, data storage, microwave absorbance, magnetic fluids, catalysis multilayer chip inductor, electromagnetic interference (EMI) suppression, gas sensing, transformer cores, antenna rods, inductors, deflection yokes, recording heads, magnetic amplifiers, radio frequency circuits, high-quality filters, rod antennas, power transformer in electronics, read/write heads for high-speed digital tapes, etc. (Kumari et al. 2015; Dumitrescu et al. 2014; Elsayed and Saba 2009; Rashad et al 2009; Lokhande et al. 2007). Furthermore, the electronic, telecommunication, lighting, energetic, and automobile industries are quickly developing nowadays and cannot be imagined without ferrite products anymore (Rashad and Ibrahim 2012). Recently, the trends of downsizing of electronic equipment and potential application in information and communication have led to fabrication of ferrite thin film (Kumbhar et al. 2014). Therefore, many kinds of techniques such as spray pyrolysis (Kumbhar et al. 2014), magnetron sputtering (Li et al. 2014a), pulsed-

✉ E. M. Elsayed
elsayed2021@gmail.com

M. M. B. El-Sabbah
mmbel_sabbah@hotmail.com

[1] Central Metallurgical Research and Development Institute (CMRDI), P.O. Box 87, Helwan 11421, Egypt

[2] Chemistry Department, Faculty of Science, Al–Azhar University, Nasr, Egypt

Table 1 pH values of different buffer solutions used for potentiodynamic polarization measurement

Buffer	pH	Composition of buffer solution
A	1.0	295 mL 0.2 M HCl + volume indicated (in 205 mL) distilled water
B	3.0	125 mL 0.2 M potassium hydrogen phthalate + volume (51 ml) 0.2 M HCl + (324 ml) distilled water
C	7.0	125 mL 0.2 M potassium hydrogen phthalate + volume indicated (in 74 mL) 0.2 M NaOH + (301 ml) distilled water
D	9.0	100 mL 0.2 M $Na_2B_4O_7.10H_2O$ (borax) + volume indicated (in 125 mL) 0.2 M KC l potassium chloride + volume indicated (in 53.5 mL) 0.2 M distilled water
E	12.0	1 M NaOH

laser deposition (Bilovol et al. 2014), sol–gel (Li et al. 2014b), chemical vapor deposition (CVD) (Shen et al. 2014), and dip coating (Sathaye et al. 2003) have been employed for ferrite film deposition. Although such methods are effective, expensive equipment limits large-scale operation. These methods usually involve elaborate and costly apparatus and complicated process. The high deposition temperature limits the option of the substrate material as well as restricts different applications of ferrite thin films. Cheaper electrochemical deposition technique has also been demonstrated to be able to fabricate textured barium ferrite films. In comparison, the electrochemical deposition technique provides not only the possibility of using low synthesis temperature but also low cost of starting materials and a high purity of the product yield (Saba et al. 2011; Gomes et al. 2004; Roy and Verma 2006; Nuli and Qin 2005; Sartale et al. 2003, 2004; Saba et al. 2012). Until now, the electrochemical performance of ferrite thin films at different pH values is not mentioned in detail in the literature. Al-Hoshan et al. (2012) studied the electrochemical performance of nickel ferrite obtained by hydrothermal method and oxygen evolution reaction. Therefore, in this paper, three nanocrystalline spinel ferrite thin films MFe_2O_4 (M=Cu, Zn, Ni) have been synthesized using electrochemical deposition technique. The changes in the crystal structure and microstructure of the produced ferrite films were investigated by X-ray diffraction (XRD) and scanning electron microscopy (SEM). Moreover, the effect of changing the pH values 1.0, 3.0, 7.0, 9.0, and 12.0 on the corrosion resistance of the ferrite samples has been evaluated. Change in the morphology and chemical composition of the films formed as a result of changing the pH was investigated by the scanning electron microscopy (SEM).

Experimental

Procedure

The Electrochemical deposition of $CuFe_2$, $NiFe_2$, or $ZnFe_2$ alloys was conducted from aqueous bath containing 0.05 M $CuSO_4{\cdot}5H_2O$, 0.0.5 M $NiSO_4{\cdot}6H_2O$, or 0.0.5 M $ZnSO_4{\cdot}7H_2O$, respectively. The source of iron in three formed alloys was 0.1 M $(NH_4)_2Fe(SO_4)_2$. All solutions were prepared immediately before each experiment by dissolving the requisite amount of analytical-grade metal sulfates in de-ionized water. The substrate used was platinum of area 1 cm^2 and the bath was stirred at 800 rpm. The alloy films were anodized using strong alkaline 1 M KOH medium. The anodization current density and time

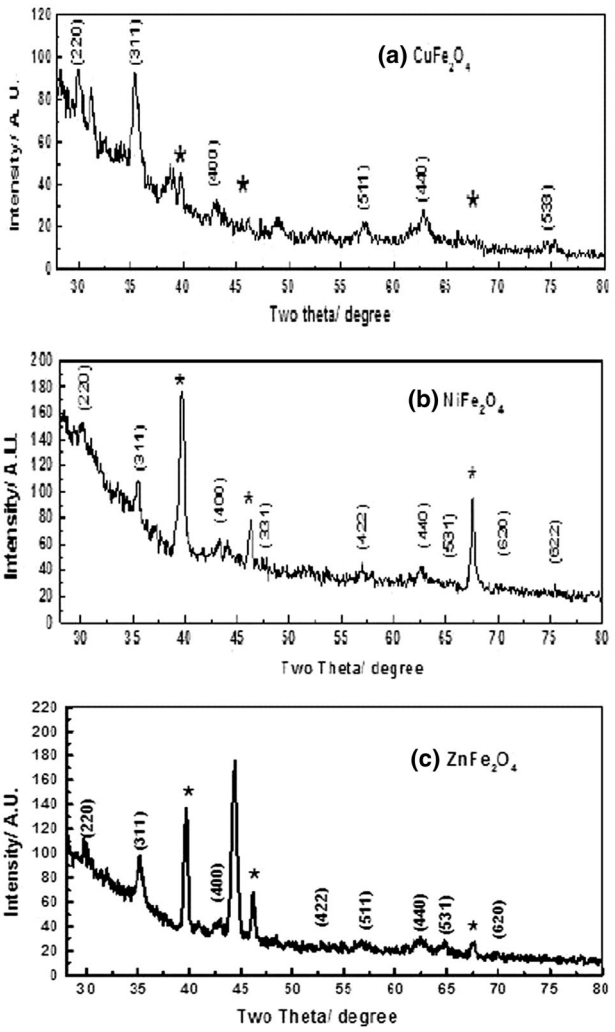

Fig. 1 XRD patterns of metal ferrites (**a** Cu ferrite, **b** Ni ferrite, and **c** Zn ferrite) annealed in air at 400 °C for 2 h where the peaks of Pt substrate are marked with *asterisk*

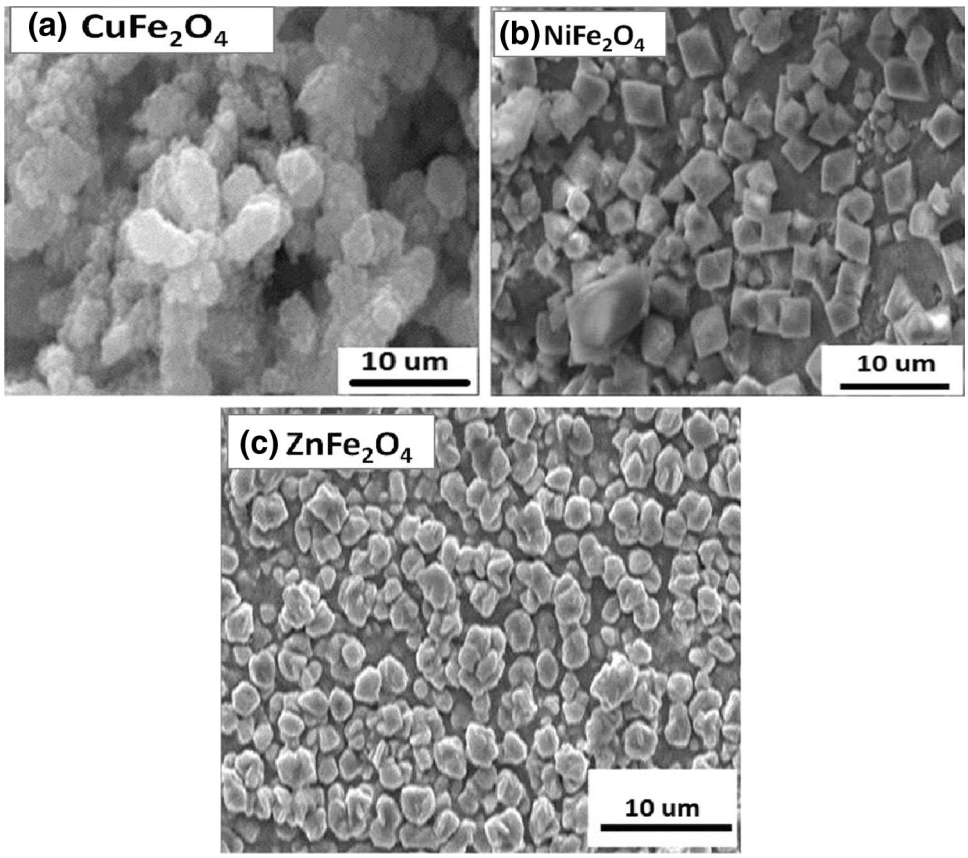

Fig. 2 SEM micrographs of metal ferrite thin films (**a** Cu ferrite, **b** Ni ferrite, and **c** Zn) ferrite from bath containing 0.05 M MSO_4 and 0.1 M $(NH_4)^2$ $Fe(SO_4)_2$ on to Pt substrate

were optimized to get well-adhered oxide films to the substrates. After anodization, the films were washed with distilled water and annealed after drying. The formed alloy film was annealed at 400 °C for 2 h.

The electrochemical cell used in potentiodynamic polarization consists of three electrodes: metal ferrite electrodes (working electrode), reference electrode Ag/AgCl, and platinum wire used as a counter electrode. The exposed area of the working electrode to solution was (1 cm^2). For the anodic and cathodic potentiodynamic polarization (Tafel plots), the entire potential scan was programmed to take place within ±250 mV of the corrosion potential. The measurements were conducted at a scanning rate of 0.2 mV/s. The potential of the metal ferrite electrodes (working electrode) was measured against Ag/AgCl (reference electrode) in buffer solution of different pH values. Table 1 lists the composition and pH values of the different used buffer solutions.

Physical characterization

The crystalline phases in the different annealed ferrite samples were investigated using X-ray diffraction (XRD) on a Brucker axis D8 diffractometer using the Cu-Kα (λ=1.5406 A°) radiation and secondary monochromator in the range 2θ from 20° to 80°. The ferrite particle morphologies with and without immersion in buffer solution at different pH values were examined by Scanning Electron Microscope (SEM) (JEOL—model JSM-5400).

Results and discussion

Synthesis of ferrite films

Figure 1a, b, c illustrates XRD patterns of ferrite films deposited on a Pt electrode from solutions containing 0.05 M of metal sulfates (MSO4 where M=Cu, Ni, and Zn, respectively) and 0.1 M ammonium ferrous sulfate $(NH4)_2Fe(SO_4)_2$ at a cathodic current density 100 mA/cm^2 for 5 min, then anodized using KOH and annealed at 400 °C for 2 h. The results revealed that well-defined spinel ferrite phase was indexed for different samples. The peaks marked with asterisks were assigned to the platinum substrate. Diffraction peak patterns corresponding to the planes (220), (311), (400), (331), (422), (440), (531), (620), and (622) of the $CuFe_2O_4$, $NiFe_2O_4$, and $ZnFe_2O_4$ were deduced. The average crystallite size of the formed film for the most intense peak (311) was estimated from the XRD data using the Debye–Scherrer formula. The crystallite size was 60, 45, and 50 nm for the formed $CuFe_2O_4$, $NiFe_2O_4$, and $ZnFe_2O_4$ films, respectively.

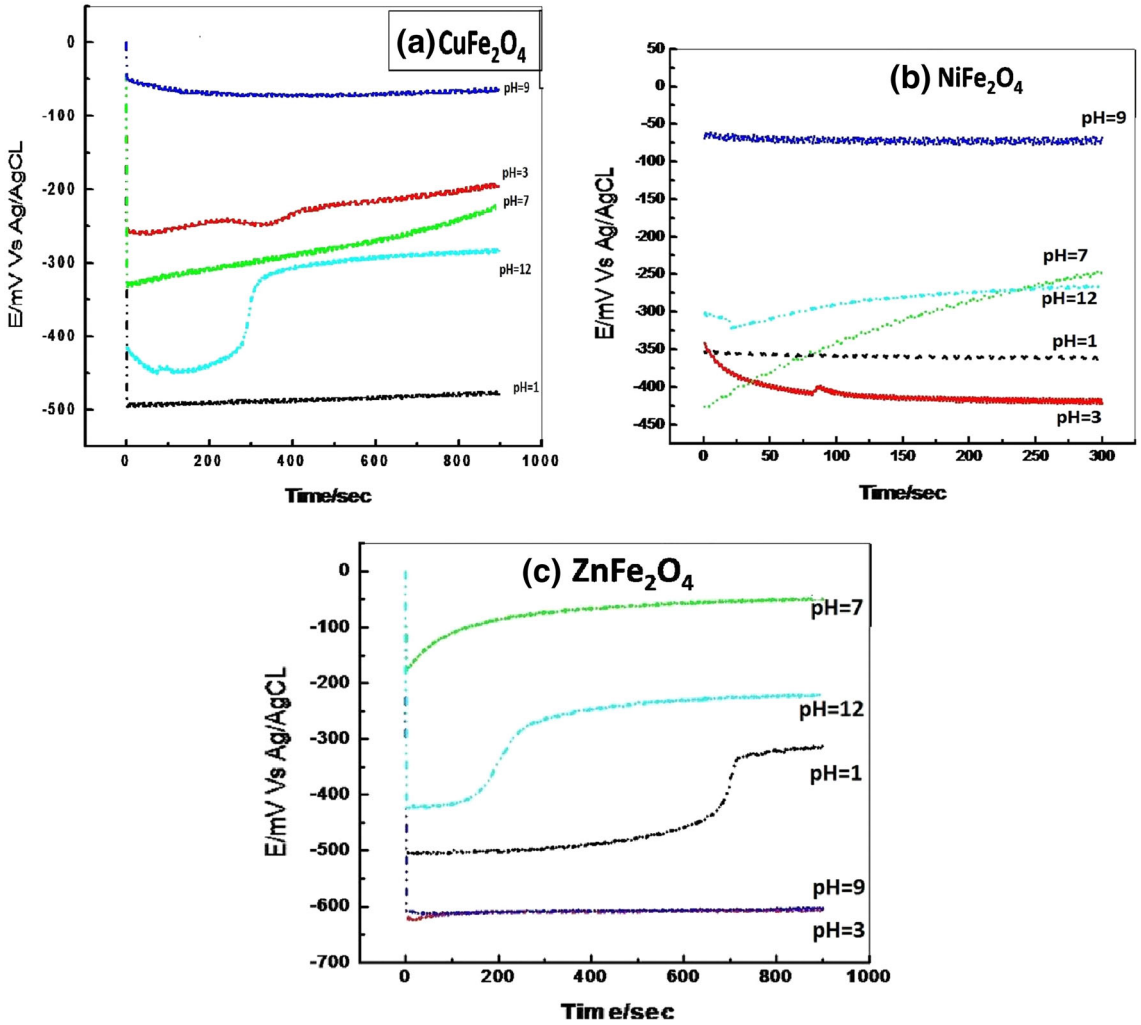

Fig. 3 Potential–time curves for metal ferrite thin films (**a** Cu ferrite, **b** Ni ferrite, and **c** Zn ferrite) in different pH solutions

Table 2 Values of E_{im} and $E_{s.s}$ (mV) for different metal (Ni, Cu, and Zn) ferrites in different pH solutions

Ferrites pH	Ni Ferrite		Cu Ferrite		Zn Ferrite	
	$E_{initial}$ (mV)	$E_{s.s}$ (mv)	$E_{initial}$ (mV)	$E_{s.s}$ (mv)	$E_{initial}$ (mV)	$E_{s.s}$ (mv)
1	−356	−361.6	−495	−480	−503.5	−316.8
3	−341	−422.3	−254.1	−190	−621.8	−609.8
7	−427.7	−249.8	−333	−218	−171.6	−52.9
9	−69.88	−77.36	−49.4	−65.48	−606.03	−599.2
12	−300	−264.8	−420	−284.1	−423	−255.05

Figure 2 shows the scanning electron micrographs of the formed spinel ferrite films. The microstructure with quasi-agglomerated spherical-like structure appeared with $CuFe_2O_4$ (Fig. 2a) with slightly random and unclear deposition, whereas the morphology of the produced $NiFe_2O_4$ film (Fig. 2b) was found to be regular cubic-like structure. However, SEM micrograph of $ZnFe_2O_4$ film was displayed as pseudo-cubic-like structure. Furthermore, it can be seen that the ferrite films were covered the whole substrate and the larger grain size of the produced films compared with the crystallite size given by the XRD patterns were observed as the results of the agglomeration of the particles.

Electrochemical performance

The way in which a metal changes its potential upon immersion in solution indicates the nature of reaction taking place at its surface. While a shift in potential in the noble

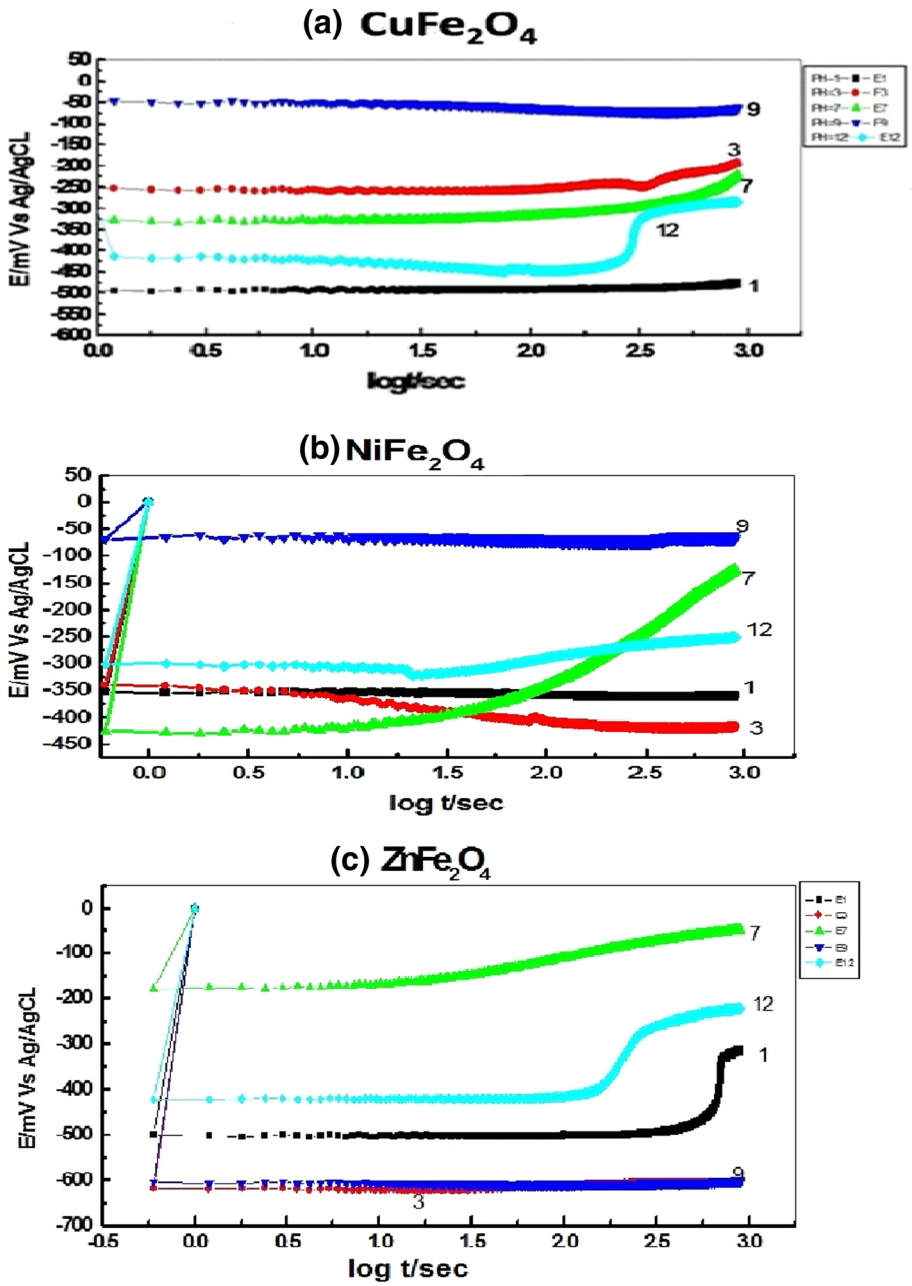

Fig. 4 Potential–log t curves for metal ferrites (**a** Cu ferrite, **b** Ni ferrite, and **c** Zn ferrite) in different pH solutions

Table 3 Values of slopes of E(mV) VS. log *t* lines and the rate of oxide film thickening (∂) (nm/log t) for corresponding Zn, Cu, and Ni ferrites in different pH solutions

Ferrites pH	Ni Ferrite		Cu Ferrite		Zn Ferrite	
	Slope	Rate (nm/log t)δ^-	Slope	Rate (nm/log *t*)δ^-	Slope	Rate (nm/log *t*)δ^-
1	10.01	0.2539	−6.93	−0.1759	6.410	0.1627
3	1.67	0.0424	−24.90	−0.6321	18.00	0.4569
7	60.00	1.5232	128.00	3.2496	28.00	0.7108
9	−1.18	−0.0299	−1.95	−0.0495	−7.62	−0.01935
12	31.01	0.7873	53.58	1.3602	4.80	0.1219

direction denotes film repair and healing, a shift in the negative direction signifies film destruction and the exposure of more of the surface electrodes to the aggressive solution. The results obtained were used in the discussion of the mechanism of oxide film growth in aerated test solutions.

The open circuit potential for Zn, Cu, and Ni ferrite electrodes as a function of time in solutions of different pH values is shown in Fig. 3, and the results are listed in Table 2. The inspection of OCP curves reveals the following arguments. It was found that at all tested pH, the OCP increases or decreases or almost constant with time until it reaches steady-state values. Solution pH normally influences the corrosion behavior of iron and its alloys by changing the stability of the oxide film, as predicted by the Pourbaix diagram (Pourbaix 1974). In the pH range from 4 to 10, the corrosion rate of iron is relatively independent of the pH of the solution. In this pH range, the corrosion rate is governed largely by the rate at which oxygen reacts with absorbed atomic hydrogen, thereby depolarizing the surface and allowing the reduction reaction to continue. For pH values below 4.0, ferrous oxide (FeO) is soluble (Mahross 2010). Thus, the oxide dissolves as it is formed rather than depositing on the metal surface to form a film. It is also observed that hydrogen is produced in acid solutions below a pH of 4, indicating that the corrosion rate no longer depends entirely on depolarization by oxygen, but on a combination of two factors (hydrogen evolution and depolarization). For pH values above about 10, the corrosion rate is observed to fall as pH is increased. For the OCP of $ZnFe_2O_4$ in higher acidic and alkaline buffer solutions (pH = 1.00 and 12.00), the initial potential E_{im} remained constant for a short time, then sharply increased in the less negative direction. However, at moderately acidic solution (pH = 3.00) and alkaline solution (pH = 9.00), the difference in potentials between E_{im} and E_{ss} was almost constant (5–12 mV). Indeed, Zn ferrite film in neutral solution (pH = 7.00) offered a good resistance where the potential shifts with time towards a noble direction. In variance, the change in the potential values with the observation that E_{ss} in pH = 1.00 is more negative than (pH = 9.00) that in the case of $CuFe_2O_4$ and $NiFe_2O_4$. In spite of that, the potentials of $CuFe_2O_4$ and $NiFe_2O_4$ films were found to decrease in the first 5.00 at pH values of 3.00 and 12.00 min indicating the dissolution of primary oxide and then moved to the passive state. On the other hand, in neutral solution (pH = 7.00), the dissolution steadily increased in the noble direction. The results deal with published before using potentiometry up to 275 °C to study of pH titrations of cobalt ferrite particles (Lefèvre and Berger 2014).

A theory for film thickening on the surface of metal and alloy based on open circuit potential measurements has been developed by Abd El-Kader and Shams El-Din (1979). The essence of the theory is based on the idea that the potential is determined by simultaneous anodic (film formation) and cathodic (oxygen reduction) couple, in which the anodic reaction is rate limiting. Presenting the data in the form of potential–log (time) curves, straight lines were obtained satisfying the following equation.

$$E = \text{constant} + 2.303(\delta^{-}/\beta)\ \log t \quad (1)$$

where (E) is the electrode potential with respect to a saturated calomel electrode, (t) is the time from the moment of immersion in solution, δ is the rate of oxide film

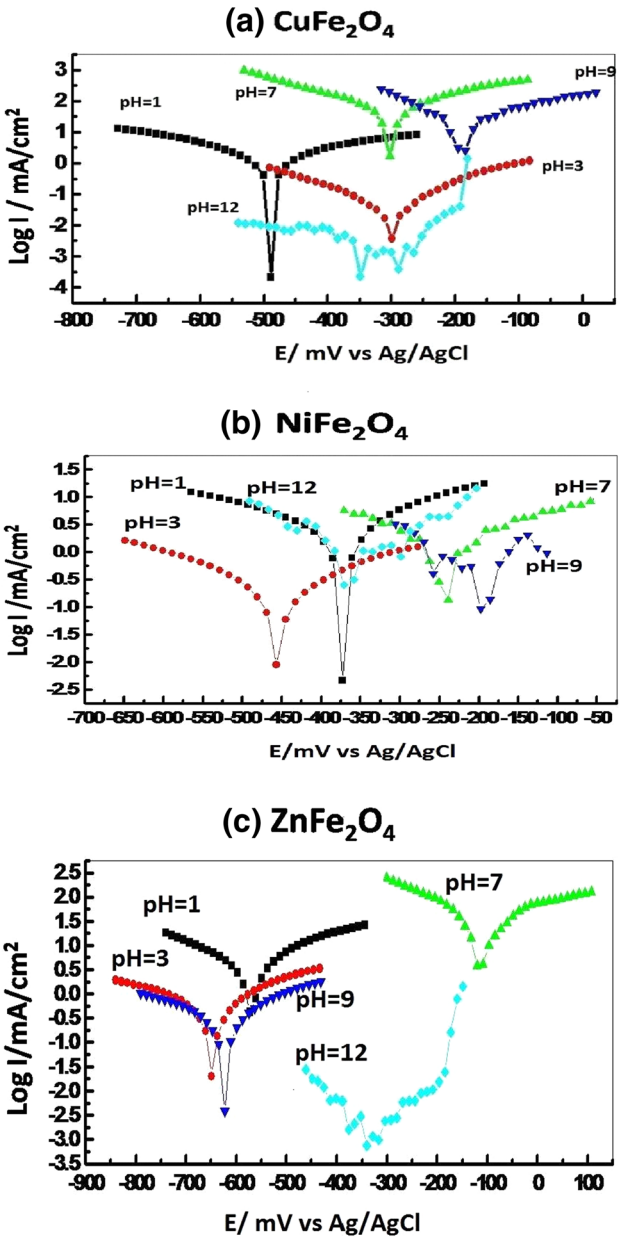

Fig. 5 Tafel plot polarization curves for metal ferrites (**a** Cu ferrite, **b** Ni ferrite, and **c** Zn ferrite) in different pH solutions

Table 4 Electrochemical Parameters of metals (Ni, Zn, and Cu) ferrites in different pH solutions

Coefficient	CR (mpy)	I_{corr} (mA/Cm^2)	$-E_{corr}$ (m V)	Bc (mV\decade)	Ba (mV\decade)	RP (Ω)	pH	Ferrites
0.9994	42.97	3.67	384.5	−360.7	265.2	14.11	1	$NiFe_2O_4$
0.9988	3.540	0.3027	469.8	−260.6	282.7	146.43	3	
0.9710	0.02455	0.00299	246.2	−162.8	345.2	45.73	7	
0.7658	0.00229	0.00017	202.8	−73.3	47.4	−558.5	9	
0.9939	0.02357	0.0020	360.7	−197.3	143.5	7.06	12	
1.000	41.2	3.524	57.6	−235.5	210.9	9.83	1	$ZnFe_2O_4$
0.9993	7.581	0.6482	651.5	−406	278.2	84.31	3	
0.9999	0.4429	0.0378	108.7	−241.0	404.7	1.41	7	
0.9959	3.386	0.2895	632.5	−288.8	189.0	139.19	9	
0.9872	18.27	1.5626	337.0	−95.6	108.8	8.52	12	
0.9974	21.43	1.8325	476.0	−262	328.9	27.01	1	$CuFe_2O_4$
0.9942	0.493	0.0421	291.1	−175.1	127.9	599.36	3	
0.9957	0.674	0.0576	280.6	−233.4	214.2	619.42	7	
0.9941	0.1601	0.01368	187.4	0.9941	138.8	1.34	9	
0.976	0.02722	0.0023	345.2	0.976	115.0	4.36	12	

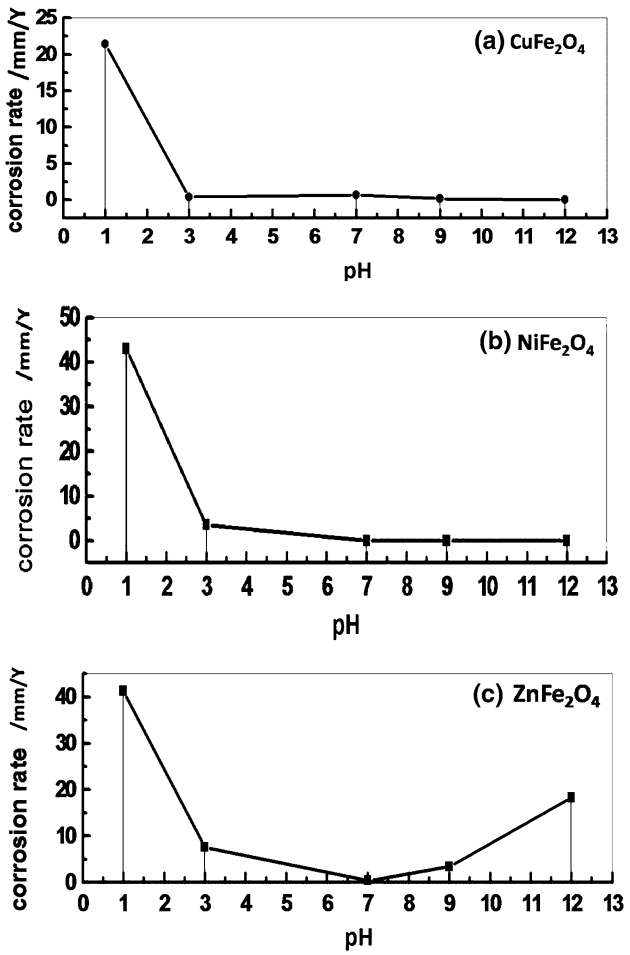

Fig. 6 Corrosion rate versus pH curves for metal ferrites (**a** Cu ferrite, **b** Ni ferrite, and **c** Zn ferrite) in different pH solutions

thickening per decade of time, and β is a constant and is given by the equation:

$$\beta = (\mathrm{nF} / \mathrm{RT})\alpha\delta^{-} \quad (2)$$

where (α) is a transference coefficient similar to that found in electrochemical kinetic rate expressions ($0.0 < \alpha < 1$), (δ^{-}) is the width of the activation energy barrier to be traversed by the ion during oxide formation, R is the gas temperature, and T is the absolute temperature. This behavior can readily be understood when one takes into consideration the physical properties of metal oxides, covering the metal surface. It is noticed from Fig. 4 and the values of (δ) in Table 3 that $ZnFe_2O_4$, $CuFe_2O_4$, and Ni Fe_2O_4 offered higher oxide film thickening (1.5232, 0.7108, and 3.2496 nm/Log t, respectively) at pH near neutral. However, the value for $ZnFe_2O_4$ was decreased at higher acidic medium (0.2539 nm/Log t) and alkaline solution (0.7873 nm/Log t). This indicates that the thickness of the formed mixed oxide films was increased with the field strength in the passive region. The obtained film may consist of a thin non-structural barrier layer next to the ferrite layer and a thicker crystalline layer next to the barrier layer. For the electrodes in the present study, the order of decrease in the rate of oxide film thickening can follow the following order:

- In higher acidic solutions, $ZnFe_2O_4 >$ Cu $Fe_2O_4 \approx$ Ni Fe_2O_4.
- In higher alkaline solutions, Ni $Fe_2O_4 > ZnFe_2O_4 >$ - Cu Fe_2O_4.
- In neutral buffer solutions, Ni $Fe_2O_4 > ZnFe_2O_4 >$ Cu Fe_2O_4.

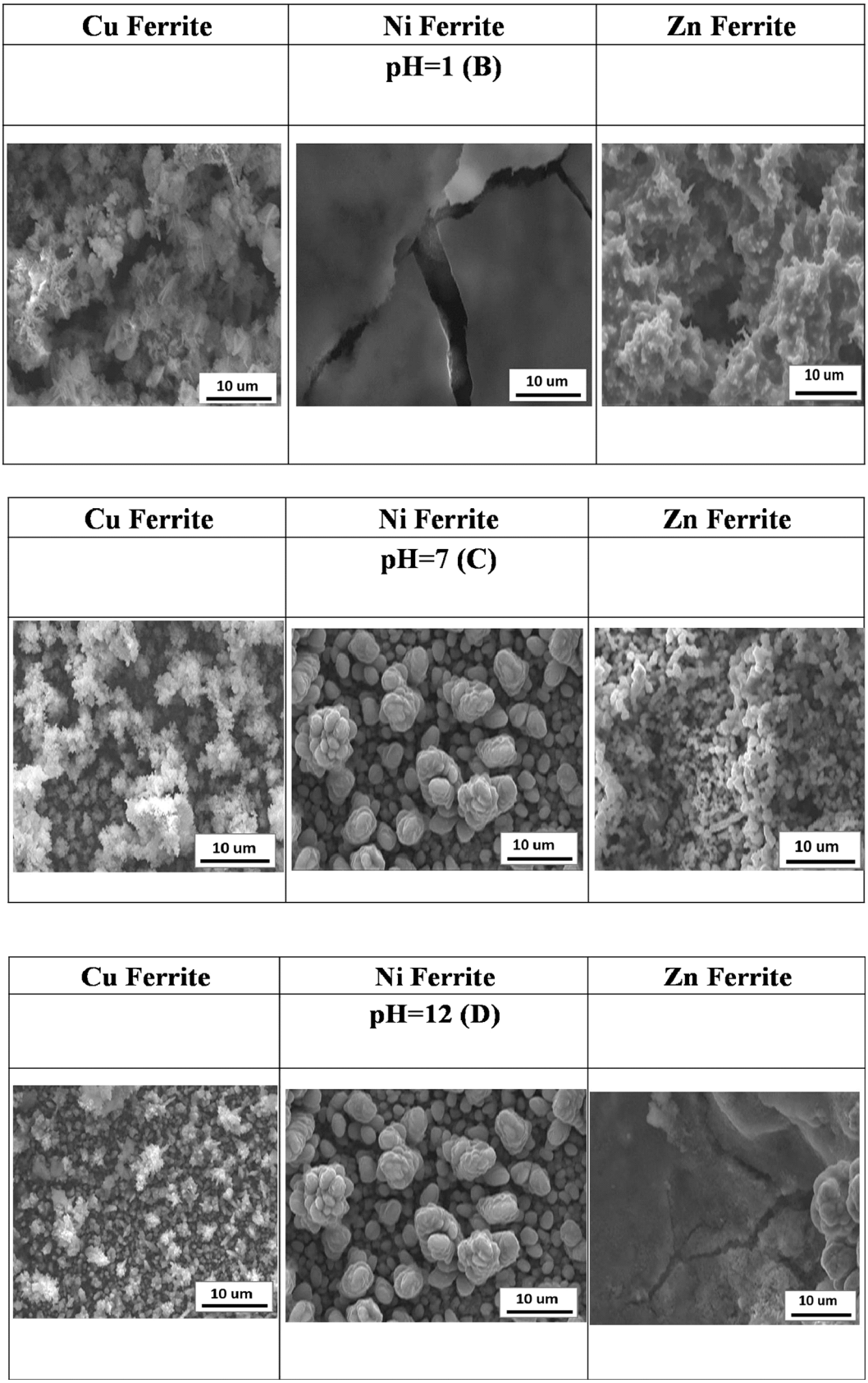

Fig. 7 SEM images of Cu, Ni, and Zn Ferrites before and after exposure to different pH solutions

Figure 5 represents Tafel plot polarization curves of different metal ferrites in buffer solution at different pH values. The corrosion kinetic parameters are listed in Table 4. The results revealed that the resistance polarization (R_p), Tafel slopes (β_a, β_c), corrosion potential ($E_{corr.}$), corrosion current density ($I_{corr.}$), and corrosion rate (C.R.) are functions of pH values. It can be seen that in buffer solutions with pH 1.00, the metal ferrites were in active state, characterized with high corrosion current density of 3.67, 3.524, and 1.8325 mA/cm^2 for Ni, Zn, and Cu ferrites, respectively. When increasing the pH from 1.00 to 3.00, I_{corr} values were sharply decreasing by $\approx$92, 82, and 98 % for Ni, Zn, and Cu ferrites, respectively. In disparity, for the above pH, ferrous oxide (FeO) is soluble. Thus, the oxide dissolves as it formed rather than depositing on the metal surface to form a film. In the absence of the protective oxide film, the metal surface is in direct contact with the acid solution, and the corrosion reaction proceeds at a greater rate than it does at higher pH values. It is also observed that hydrogen is produced in acid solutions below a pH of 3.00, indicating that the corrosion rate no longer depends entirely on depolarization by oxygen, but on a combination of the two factors (hydrogen evolution and depolarization *n*) (Yadla et al. 2012). Furthermore, when the pH of the buffer increased to neutral and alkaline solutions (pH = 7, 9 and 12), there are two different behaviors for metal ferrites. For Ni and Cu ferrites, stable passive state was observed which may be due to mixed oxide layers. While in the case of Zn ferrite, the stable passive state was observed only at neutral solution. But there was a sharp rise at moderate and high alkaline solution. For pH values above about 3.00 for Ni and Cu ferrites, the corrosion rate is observed to fall as pH is increased. This is believed to be due to the increase in the rate of the reaction of oxygen with $Fe(OH)_2$, $Ni(OH)_2$, and $Cu(OH)_2$ (hydrated metal) in the oxide layer to form the more protective Fe_2O_3 with Ni and Cu oxides. But for Zn ferrite, the metal oxide or hydroxide, it is thermodynamically unstable in the presence of water in aqueous solutions and tends to dissolve with the evolution of hydrogen in acid and alkaline solutions. Figure 6 gives a clear idea of the behavior of the relationship between the corrosion rate and pH. As a result of these experiments, we recommend to use safely Ni and Cu ferrites in neutral and alkaline atmospheres, but Zn ferrite only in neutral medium.

Figure 7 illustrates the morphology of the surface of Zn, Cu, and Ni ferrites after exposure to different pH solutions. The morphology of the surface of Zn, Cu, and Ni ferrites after immersion in buffer solutions at pH = 1.00. It is clear that that the surface was severely damaged at pH = 1.00 for different ferrites. However, the microstructure of the formed ferrites after immersion in buffer solution at pH 12 was presented damaged for Zn ferrite. In contrast, the corrosion rates of $NiFe_2O_4$ and $CuFe_2O_4$ were very low at a high pH value of 12. In comparison, the morphology of the formed three ferrite films indicated that the values of corrosion rate were very low in the neutral solution at pH 7.

Conclusions

The results are summarized as follows:

- Nanocrystalline metal ferrite MFe_2O_4 (M=Cu, Zn, and Ni) thin films have been synthesized via electrodeposition–anodization process.
- The crystallite sizes of the produced films were in the range between 45 and 60 nm.
- The microstructure of the formed $CuFe_2O_4$, $ZnFe_2O_4$, and $NiFe_2O_4$ thin films appeared as quasi-agglomerated spherical-like structure, regular cubic-like structure, and pseudo-cubic-like structure, respectively.
- The open circuit potential indicates that the initial potential E_{im} of $ZnFe_2O_4$ thin films remained constant for a short time, then sharply increased in the less negative direction in acidic and alkaline media compared with Ni and Cu ferrites films.
- Tafel plot polarization curves of different metal ferrite thin films at different pH values revealed that the resistance polarization (R_p), Tafel slopes (β_a, β_c), corrosion potential ($E_{corr.}$), corrosion current density ($I_{corr.}$), and corrosion rate (C.R.) are functions of pH values.
- The values of the corrosion current density I_{corr} was higher for the $ZnFe_2O_4$ films at different pH values of 1 and 12 compared with those of $NiFe_2O_4$ and $CuFe_2O_4$ which were higher only at pH value 1.
- The corrosion rate was very low for the three ferrite films when immersion in the neutral medium.
- The surface morphology recommended that Ni and Cu ferrite films were safely used in neutral and alkaline media, whereas Zn ferrite film was only used in neutral atmospheres.

References

Abd El-Kader JM, Shams El-Din AM (1979) Film thickening on Nickel in aqueous solution in relation to anion type and concentration. Br Corros J 14:40–45

Al-Hoshan MS, Singh JP, Al-Mayouf AM, Al-Suhybani AA, Shaddad MN (2012) Synthesis, physicochemical and electrochemical properties of Nickel ferrite spinels obtained by hydrothermal method for the oxygen evalution reaction (OER). Int J Electrochem Sci 7:4959–4973

Bilovol V, Pampillo LG, Saccone FD (2014) Study on target–film structural correlation in thin cobalt ferrite films grown by pulsed laser deposition technique. Thin Solid Films 562:218–222

Dumitrescu AM, Borhan AI, Iordan AR, Dumitru I, Palamaru MN (2014) Influence of chelating/fuel agents on the structural features, magnetic and dielectric properties of Ni ferrite. Powder Technol 268:95–101

Elsayed EM, Saba AE (2009) Preparation of standard copper ferrite thin film from aqueous solution. Steel Grips 7(2):137–141

Gomes E, Pane S, Valles E (2005) Magnetic composites CoNi-barium ferrite prepared by electrodeposition. Electrochem Commun 7:1225

Kumari N, Kumar V, Khasa S, Singh SK (2015) Chemical synthesis and magnetic investigations on Cr3b substituted Zn ferrite super paramagnetic nanoparticles. Ceram Int 41(1):1907–1911

Kumbhar SS, Mahadik MA, Mohite VS, Rajpure KY, Bhosale CH (2014) Synthesis and characterization of spray deposited Nickel-Zinc ferrite thin films. Energy Procedia 54:599–605

Lefèvre G, Berger G (2014) Potentiometry up to 275 °C: example of pH titrations of cobalt ferrite particles. J Colloid Interface Sci 430:12–17

Li L, Wang R, Tu X, Peng L (2014a) Structure and static magnetic properties of Ti-substituted NiZnCo ferrite thin films synthesized by the sol–gel process. J Magn Magn Mater 355:306–308

Li L-Z, Yu Z, Lan Z-W, Sun K, Guo R-D (2014b) Effects of annealing temperature on the structure and static magnetic properties of NiZnCo ferrite thin films. J Magn Magn Mater 368:8–11

Lokhande CD, Kulkarni SS, Mane RS, Han S-H (2007) Copper ferrite thin film: single-step non-aqueous growth and properties. J Cryst Growth 303(2):387–390

Mahross MH (2010) Corrosion Inhibition of some metals in aqueous media using some friendly environmental inhibitors. Ph D thesis University of AL-Alzhar Egypt

Nuli Y-N, Qin QZ (2005) Nanocrystalline transition metal ferrite thin films prepared by an electrochemical route for Li-ion batteries. J Power Sources 142(1–2):292–297

Pourbaix M (1974) Atlas of electrochemical equilibrium in aqueous solutions. National Association of Corrosion Engineers Houston Texas 307–321

Rashad MM, Ibrahim IA (2012) Structural, microstructure and magnetic properties of strontium hexaferrite particles synthesised by modified coprecipitation method. Mater Technol 27(4):309–314

Rashad MM, Elsayed EM, Moharam MM, Abou-Shahba RM, Saba AE (2009) The structure and magnetic properties of $Ni_xZn_{1-x}Fe_2O_4$ nanoparticles prepared through Co-precipitation method. J Alloys Compd 486:759–767

Roy MK, Verma HC (2006) Magnetization anomalies of nanosize zinc ferrite particles prepared using electrodeposition. J Magn Magn Mater 306:98–102

Saba AE, Elsayed EM, Moharam MM, Rashad MM, Abou-Shahba RM (2011) Structure and magnetic properties of $Ni_x\ Zn_{1-x}\ Fe_2O_4$ thin films prepared through electrodeposition method. J Mater Sci 46(10):3574–3582

Saba AE, Elsayed EM, Moharam M, Rashad MM (2012) Electrochemical synthesis of nanocrystalline $Ni_{0.5}Zn_{0.5}Fe_2O_4$ thin film from aqueous sulfate bath. ISRN Nanotechnol 2012:1–8, Art ID 532168. doi:10.5402/2012/532168

Sartale SD, Lokhande CD, Muller M (2003) Electrochemical synthesis of nanocrystalline $CuFe_2O_4$ thin films from non-aqueous ethylene glycol medium. Mater Chem Phys 80(1):120–128

Sartale SD, Lokhande CD, Giersig M, Ganesan V (2004) Novel electrochemical process for the deposition of nanocrystalline $NiFe_2O_4$ thin films. J Phys Condens Matter 16:773–784

Sathaye SD, Patil KR, Kulkarni SD, Bakre PP, Pradhan SD, Sarwade BD, Shintre SN (2003) Modification of spin coating method and its application to grow thin films of cobalt ferrite. J Mater Sci 38:29–33

Shen L, Althammer M, Pachauri N, Loukya B, Datta R, Iliev M, Bao N, Gupta A (2014) Epitaxial growth of spinel cobalt ferrite films on $MgAl_2O_4$ substrates by direct liquid injection chemical vapor deposition. J Cryst Growth 390:61–66

Yadla SV, Sridevi V, Lakshmi MVVC, Kumari SPK (2012) A review on corrosion of metals and protection. International Journal of Engineering Science & Advanced Technology 2(3):637–644